

Into Arid Unknowns: Projecting Drought Over the Northeastern United States Using NEX-GDDP-CMIP6

Immanuel Chas Bissell

Advisor: Prof. Kai Chen

Second Reader: Prof. Mark Brandon

1 May 2024

A Senior Essay presented to the faculty of the Department of Earth and Planetary Sciences, Yale University, in partial fulfillment of the Bachelor's Degree.

In presenting this essay in partial fulfillment of the Bachelor's Degree from the Department of Earth and Planetary Sciences, Yale University, I agree that the department may make copies or post it on the departmental website so that others may better understand the undergraduate research of the department. I further agree that extensive copying of this thesis is allowable only for scholarly purposes. It is understood, however, that any copying or publication of this thesis for commercial purposes or financial gain is not allowed without my written consent.

Immanuel Chas Bissell
May 2024

Contents

Abstract	3
1. Introduction and Background	4
2. Materials and Methods	9
2.1 Study Area	9
2.2 Data and Models	10
2.3 Drought Analysis	13
3. Results	18
3.1 Historical Comparison and Validation	18
3.2 Long-term SPI and SPEI Record	21
3.3 Drought Frequency and Magnitude Increase Over Time	23
3.4 Geographic Spread of Drought	26
4. Discussion	29
5. Conclusion	32
Acknowledgments	33
References	34
Appendix	43

Abstract

Drought is among the costliest and deadliest natural disasters. Understanding the global changes in drought due to anthropogenic global warming is of environmental, economic, and societal importance. This study uses downscaled global climate model output from the Coupled Model Intercomparison Project (CMIP6) to project the Standardized Precipitation Evapotranspiration Index (SPEI), a meteorological drought index, across the northeastern United States. SPEI is computed for low and high emissions scenarios and calculated across 6-month and 12-month timescales. We find that downscaled CMIP6 output demonstrates agreement with historical observations across a range of climatic variables. Our findings reveal that when compared to drought indices based solely on precipitation, SPEI more accurately portrays the effects of global warming on drought patterns. SPEI projections demonstrate that under high emissions scenarios, all severity categories of drought in the study area experience heightened frequency and duration, both temporally and geographically, in contrast to low emissions scenarios, especially in Eastern Pennsylvania and Upstate New York. Together, these results affirm the need for serious and urgent action on climate change mitigation and establish a scalable path to further studies.

1. Introduction and Background

Drought is a period of water shortage within an environmental or social system. The impacts of such periods are highly variable: water scarcity is a common occurrence within climatic variations and occurs in nearly all regions of the globe but, depending on frequency, severity, and duration, can lead to severe climate events that impact ecological, socioeconomic, and agricultural conditions. Large-scale droughts, referred to as megadroughts once they become multidecadal, have long gripped the anthropological imagination due to their association with the collapse of civilizations from the Ancestral Pueblo to the Khmer Empire (Cook et al., 2016). In the more recent past, the 1930s American Prairie Dust Bowl, an environmental disaster that led to wide-scale migration across the continent and reshaped the American population, was largely driven by persistent drought from 1930-1936 (Long and Siu, 2018; Schubert et al., 2004). Today, drought is the second most expensive natural disaster in the United States and has high human costs—between 1980 and 2020 drought-related damages totaled \$250 billion and killed nearly 3000 people (Ault, 2020; NOAA, 2020). Indeed, 18 of the 20 years between 2002 and 2022 saw drought-related agricultural losses of over a billion dollars in the U.S., with an average loss of \$6.97 billion (Leeper et al., 2022).

The severity of these impacts largely depends on the timescales and regions affected by drought. Prolonged water shortages can alter the availability of combustible fuel for forest fires, impacting acreage burned, heat of combustion, and frequency of fires (Leeper et al., 2022).

About 40% of freshwater withdrawals in the U.S. are used to cool power plants, and thus seemingly marginal decreases in water supply can stress electrical grids, leading to increased power outages and decreased industrial productivity (Pacsi et al., 2013; Scoriah et al., 2012).

Such climatic changes can also have serious impacts on human health. Water shortages can result

in substantial crop losses and increased dependence on stagnant water sources, and can trigger secondary effects such as algal blooms, shifts in the distribution of disease-carrying vectors like mosquitoes and ticks, and a heightened prevalence of mental health issues (Sugg et al., 2020). In extreme cases, water shortages and famine can lead to increased human conflict and involuntary migration (Sun et al., 2019). Because drought can occur on time scales ranging from weeks to years, acute consequences can compound and increase in severity due to their interplay.

As such, projecting the future spatial extent and temporal frequency of drought is of social, political, and economic interest. This is especially true in light of anthropogenic climate change. Regional warming and drying under high emissions scenarios have been projected to increase the incidence of megadrought across China and the Southeast U.S. (Ault et al., 2016; Leng et al., 2015). In one representative study of East Africa, drought-prone areas were projected to increase by up to 54% under Representative Concentration Pathway (RCP) 8.5 (Haile et al., 2020). Globally, the proportion of land and human population experiencing extreme drought by the end of the century could more than double, with more than two-thirds of global land experiencing decreases in water storage (Pokhrel et al., 2021; Schwalm et al., 2017). Moreover, heightened severity and prolonged duration of droughts have the potential to impact human biogeography significantly. Since 2008, an average of 22.5 million people have been displaced annually due to climate-related events (Bower et al., 2015). Climatic conditions unprecedented in recent human history will likely exacerbate involuntary migration (Haile et al., 2020). But while the critical importance of understanding future drought is clear, there is still no universally accepted definition of what exactly constitutes a drought.

Definitions of drought are generally organized under four categories depending on the impact under consideration: *meteorological drought*, *agricultural drought*, *hydrological drought*,

and *socioeconomic drought*. Myriad drought indices have been developed to characterize and quantify the severity and duration of drought in each category—a comprehensive review by Zargar et al. (2011), for example, enumerated more than 91 unique indices. *Meteorological drought* usually describes the degree of dryness within a local weather system resulting from some combination of precipitation deficiency and increased evaporation through changes in temperature, wind, and radiation. Because other categories of drought regularly follow from arid meteorological conditions, and because the number of variables required to calculate meteorological water balances is substantially lower than that required for terrestrial water storage or agricultural water availability, *meteorological drought* is an excellent basis for future drought projection.

A milestone in the quantification of meteorological drought was the development of the Palmer Drought Severity Index (PDSI). Initially conceived by Palmer in 1965, PDSI allows for the characterization of both abnormally wet and dry periods by employing a primitive water balance equation that includes precipitation, evaporation, and runoff (Alley, 1984; Palmer, 1965; Wells et al., 2004). The index then employs weighing factors termed “duration factors” to adjust for regional and seasonal differences. Though PDSI became the standard meteorological drought index in the decades following its introduction and is still widely used today, it has several distinct deficiencies (Vicente-Serrano et al., 2012). These include often generating a slightly bimodal distribution with peaks outside of the categories considered “near normal,” not sufficiently allowing for calculation at different time scales, and producing values classified as “extreme” (> 4 or < -4) more than 15% of the time (Schrier et al., 2006; Wells et al., 2004). Perhaps most significantly, the duration factors used in the computation were empirically derived from limited data gathered from the American Great Plains. These factors led to poor

performance under different climatic regimes and unreliable comparisons between locations and time periods (Sousa et al., 2011; Vicente-Serrano et al., 2010). In response to these criticisms, a revised version of the PDSI was proposed by Wells (2004) called the self-calibrated PDSI (scPDSI). This updated metric reduced the frequency of extreme events and adjusted the duration factors to be calculated from local data (Sousa et al., 2011).

Nevertheless, the lack of computability across distinct time scales is a significant disadvantage of PDSI-based metrics and led to the development of alternative indices. One widely used index proposed by McKee et al. (1993) is the standard precipitation index (SPI). SPI is calculated purely from precipitation records and can be adjusted across timescales to allow for the modeling of water supplies from short-term soil moisture to long-term water table balances. Computation involves the standardization of long precipitation time series (>30 months) using, most commonly, gamma or Pearson type III distributions (W. Wang et al., 2021). However, a criticism of this index is that it is essentially a fit of precipitation data (Vicente-Serrano et al., 2012; Vicente-Serrano and López-Moreno, 2005). SPI assumes that precipitation is the factor with the most variability and there are no long-term trends in evaporative factors like radiation and temperature. These assumptions are clearly not sufficient for projection under long-term warming scenarios.

Correspondingly, Vicente-Serrano et al. (2010) developed the Standardized Precipitation Evapotranspiration Index (SPEI). This index is calculated in much the same way as SPI but is based on a water balance between precipitative input and evaporative loss rather than just precipitation. This metric has been used in a diverse set of contexts and is robust at various timescales (Feng and Su, 2019; Mallya et al., 2016; Vicente-Serrano et al., 2012; W. Wang et al.,

2021). These factors make SPEI an appropriate metric for projecting drought under future climatic scenarios across a diverse range of locations.

This essay uses SPI and SPEI to project drought under high and low emissions scenarios in a section of the American Northeast centered in Connecticut using a set of downscaled model outputs from the Coupled Model Intercomparison Project Phase 6 (CMIP6). This downscaled dataset allows for long-term assessment at a higher resolution than has been done in any previous drought projections from CMIP6 output. In doing so, these results not only report on the future state of water resources in the Eastern U.S. but also set a scalable and replicable path to future studies of water abundance across wider geographic extents.

2. Materials and Methods

2.1 Study Area

The study area for this essay comprises a $\sim 330 \text{ km} \times 500 \text{ km}$ grid centered at 41.5° N , 72° W spanning between $43^\circ 0' - 40^\circ 0' \text{ N}$ and $69^\circ 15' - 75^\circ 15' \text{ W}$ (Figure 1). This region fully contains Connecticut, Massachusetts, and Rhode Island, as well as parts of Vermont, New Hampshire, New York, New Jersey, and Pennsylvania. This equates to an area covering $\sim 1.6 \times 10^5 \text{ km}^2$ with an estimated population of ~ 38 million people (CIESIN, 2018). The topography is fairly low and uniform across the study area. Climatic regimes are also fairly consistent across the region as well, with 50-year historical Köppen climate types ranging from humid Subtropical (Köppen Cfa) in the southern end to warm-summer humid continental (Köppen Dfb) in the North (Kottek et al., 2006).

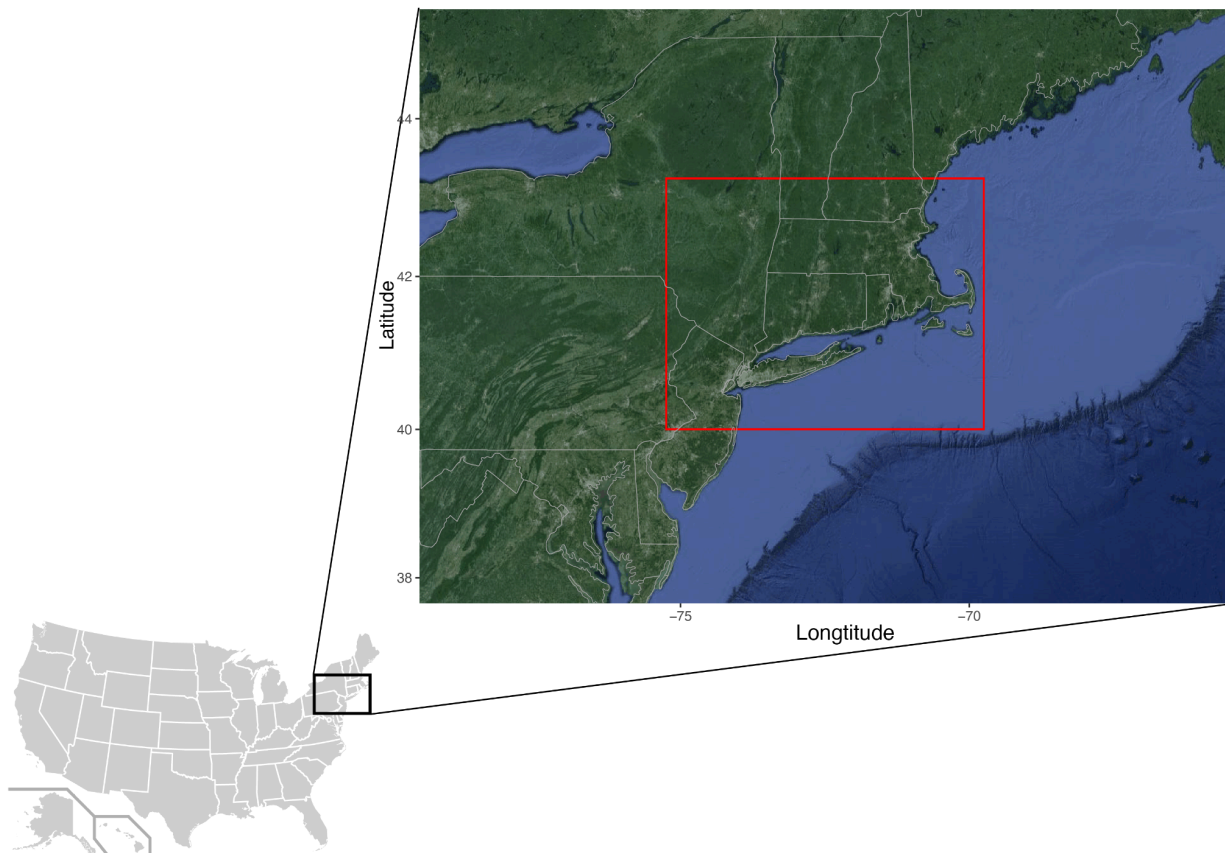


Figure 1. The geographic extent of the study region is shown in context by the red bounding box. Satellite imagery was sourced from Google Maps API (retrieved March 31, 2024).

2.2 Data and Models

The climate data used in this study are from the NASA Earth Exchange Global Daily Downscaled Projections (NEX-GDDP). These are a set of downscaled daily climate scenarios derived from CMIP6. The dataset provides output from 35 global climate models for eight climatic variables across five Shared Socioeconomic Pathways (SSPs; Thrasher et al., 2022). The SSPs are designed to represent a range of land use and emissions scenarios reflective of future economic growth, governance, and climatic mitigation success (O'Neill et al., 2016; van Vuuren et al., 2012). The scenarios are then used in the generation of Representative Concentration Pathways (RCPs) based on the ensuing greenhouse gas emissions and radiative forcing ability.

The NEX-GDDP dataset consists of CMIP6 output that has been statistically downscaled using the bias correction/spatial disaggregation (BCSD) method, which enhances resolution and spatial reliability (Thrasher et al., 2022). While this method proves robust in many scenarios, it operates under the assumption of consistent climatic patterns over time and might underestimate extreme climatic events in distant future periods (Jang and Kavvas, 2015; Wood et al., 2004; Zhang et al., 2019). As such, additional projection should be done as alternatively downscaled outputs become available. Nevertheless, the BCSD technique incorporates variable bias correction by comparing regional observations from a relevant historical period through a quantile mapping approach, and this inclusion aids in addressing some variability (Thrasher et al., 2022). This statistical downscaling method allows for the CMIP6 output to be brought to a final resolution of $0.25^\circ \times 0.25^\circ$ degrees ($\sim 27 \text{ km} \times 27 \text{ km}$) across all models, which is a higher resolution than that used in previous CMIP6 drought projections.

For this study, six models were chosen based on their usage and reliability in past hydrometeorological and drought-related studies (Table 1; Cook et al., 2020; T. Wang et al., 2021).

Table 1. Global Climate Models (GCMs) used in this study.

Model	Institute	Country	References
BCC-CSM2-MR	Beijing Climate Center	China	Wu et al. (2018)
CanESM5	Canadian Centre for Climate Modelling and Analysis	Canada	Swart et al. (2019)
GFDL-ESM4	National Oceanic and Atmospheric Administration	USA	Krasting et al. (2018)
GISS-E2-1-G	Goddard Institute for Space Studies	USA	NASA (2018)
IPSL-CM6A-LR	Institut Pierre-Simon Laplace Climate Modelling Centre	France	Boucher et al. (2018)
MIROC6	Japan Agency for Marine-Earth Science and Technology	Japan	Tatebe and Watanabe (2018)

Precipitation, maximum temperature, minimum temperature, and downwelling radiation were obtained for each model and used to calculate potential evapotranspiration and drought metrics. The historical condition for each variable spanned 1979-2014. SSP1-2.6 (radiative forcing 2.6 W/m²), in which warming is kept below 2°C by 2100 was included as the low emissions scenario (T. Wang et al., 2021). SSP5-8.5 (radiative forcing 8.5 W/m²) represents a ‘worst case scenario’ in which greenhouse gas emissions continue unencumbered and warming rises by ~4°C by 2100. Both future scenarios were projected for 2015-2100.

In addition to assessing the output from each model individually, all CMIP6 models were assembled into an ensemble average to account for uncertainty in each individual model. In general, multi-model ensembles have been shown to produce superior results to individual models (Crawford et al., 2019; Ramesh and Goswami, 2014; Tebaldi and Knutti, 2007). The ensemble average was calculated as the arithmetic mean of the six individual models calculated for each grid point at each point in time. This method allows for the ensemble average data to be used as input into further analyses in the same way as individual models. Though other

techniques for the development of model ensembles, such as random forest and neural network methods, are more accurate in several contexts, an arithmetic mean is sufficient for this study as (1) arithmetic ensemble means have given satisfactory results in a variety of studies using CMIP6 output for projection and historical state reconstruction (Masud et al., 2021; Mishra et al., 2020; Ngoma et al., 2021), and (2) the variables that would benefit most from uncertainty correction through model aggregation, such as precipitation, often show such high variability that there is no marked increase with more complicated methods, while the variables modeled best by GCMs, such as temperature, also do not, or need not, show substantial increases in accuracy (Crawford et al., 2019).

Historical data for comparison and calibration was obtained from gridMET (Abatzoglou, 2013), downloaded using the ‘climateR’ package in R. This dataset contains high-resolution (1/24th degree) climatic data from 1979 to the present day. All climatic variables available from NEX-GDDP are available from gridMET, as well as several derived variables, including reference evapotranspiration computed using the Penman-Montieth equation. Importantly, this allowed for the comparison and calibration of both primary and derived variables used in the analysis here with the historical record.

2.3 Drought Analysis

Both SPI and SPEI were employed as drought indices for this study and were computed using the ‘SPEI’ package in R. SPI is the simpler of the two metrics and involves, in essence, a standardized fit of precipitation data. Following McKee et al. (1993), first, a probability density function is fitted over the precipitation dataset. An incomplete gamma probability density function (as shown here) was used for this study

$$g(x) = \frac{1}{\beta^\alpha \Gamma(\alpha)} x^{\alpha-1} e^{-\frac{x}{\beta}} \quad (1)$$

where $x > 0$, α and β are the shape and scale parameters, respectively, x is the precipitation, and Γ is the gamma function. The probability distribution is then given by

$$G(x) = \int_0^x g(x) dx = \frac{1}{\beta^\alpha \Gamma(\alpha)} \int_0^x x^{\alpha-1} e^{-x/\beta} dx \quad (2)$$

This formulation allows SPI to be simply calculated as

$$SPI = S \frac{c_0 + c_1 t - c_2 t^2}{1 + d_1 t + d_2 t^2 + d_3 t^3} \quad (3)$$

with

$$t = \sqrt{\ln \left(\frac{1}{G(x)^2} \right)} \quad (4)$$

where x is precipitation, S is the positive or negative cumulative probability distribution coefficient reflecting the value of $G(x)$, and $c_0, c_1, c_2, d_1, d_2, d_3$ are fitting constants. This standardization transforms precipitation series to have an average at 0 with a standard deviation of 1 and allows for assessment of both particularly wet and dry periods.

As mentioned above, SPI does not account well for long-term trends and short-term variability non-precipitation variables because these elements are left out of its computation. SPEI, owing to its integration of evapotranspiration, was thus included as the primary drought index in this study. Its computation follows a similar trajectory to SPI but uses a water balance as the primary time series rather than just precipitation. For any given month with precipitation P_i and potential evapotranspiration PET_i , the water balance is given by

$$D_i = P_i - PET_i \quad (5)$$

PET was calculated here using the modified Hargreaves equation (Droogers and Allen, 2002).

This method develops on the original Hargreaves equation outlined in Hargreaves (1994) and Hargreaves et al. (1985) by correcting for ET_0 each month by using precipitation as a proxy for irradiation

$$ET_0 = 0.0013 \cdot 0.408RA \cdot (T_{avg} + 17.0) \cdot (TD - 0.0123P)^{0.76} \quad (6)$$

where P is precipitation in mm per month, RA is the extraterrestrial radiation in $MJ m^{-2} d^{-1}$, T_{avg} is the average daily temperature in $^{\circ}C$, and TD is the temperature range between the daily maximum and minimum temperatures in $^{\circ}C$. The modified Hargreaves equation is in better agreement with the Penman-Monteith equation, which is the current standard for estimating *PET* but has substantially higher data input requirements (Droogers and Allen, 2002).

Once *PET* is computed, water balances can be estimated through the precipitation-evaporation difference and summed across different time scales. A three-parameter log-logistic model was selected to standardize the water balance time series, as was done originally by Vicente-Serrano et al. (2010), with probability density function

$$f(x) = \frac{\beta}{\alpha} \left(\frac{x - \gamma}{\alpha} \right)^{\beta-1} \left[1 + \frac{(x - \gamma)^{\beta}}{\alpha} \right]^{-2} \quad (7)$$

in which α , β , and γ are the scale, shape, and origin parameters, respectively and D values are in the range $(\gamma > D < \infty)$. The probability distribution is then given by

$$F(x) = \left[1 + \left(\frac{1}{x - \gamma} \right)^{\beta} \right]^{-1} \quad (8)$$

With this distribution, SPEI is computed as

$$SPEI = W - \frac{c_0 + c_1W + c_2W^2}{1 + d_1W + d_2W^2 + d_3W^3} \quad (9)$$

with

$$W = \sqrt{-2 \ln(P)} \quad (10)$$

where P is the probability of exceeding a calculated value of D given by $P = 1 - F(x)$. $c_0, c_1, c_2, d_1, d_2, d_3$ are all constants derived from the distribution above. For this study, unbiased probability-weighted moments were selected as the method for parameter fitting. Because this formulation standardizes the mean and standard deviation, SPEI can be compared across space and time while also accounting for long-term evaporative trends (Vicente-Serrano et al., 2010). As with SPI, water balances are transformed to have an average of 0 with a standard deviation of 1, in which negative and positive values signify a water deficit and abundance, respectively.

Each index was calculated at 1-month, 6-month, and 12-month intervals to assess drought at different time scales. Because both SPI and SPEI follow a similar standardization procedure, the indices are comparable. The severity of drought under both indices (Table 2) was classified using thresholds suggested by the WMO (2012) and Zeng et al. (2022).

Table 2. Drought classification thresholds used in this study, based on suggestions by the WMO (2012).

Drought Severity Classification	Threshold
No drought	$SPI/SPEI > -1$
Moderate	$- 1.5 \leq SPI/SPEI \leq - 1$
Severe	$- 2 \leq SPI/SPEI \leq - 1.5$
Extreme	$SPI/SPEI \leq - 2$

For further analysis, 6-month and 12-month time intervals were chosen as these periods highlight the catastrophic effects of drought better than short-term analyses and have been used in similar previous studies (Haile et al., 2020; Touma et al., 2015; T. Wang et al., 2021). The selection of these two timescales also speaks to two differing impacts of drought. SPEI-6 has been shown to correlate with root zone soil moisture, and thereby is more pertinent to agricultural considerations, while SPEI-12 has been found to better reflect water-table and groundwater levels (Kumar et al., 2016; Leelaruban et al., 2017; Pyarali et al., 2022; Secci et al., 2021). Drought measured by these indices was classified using run theory, a probabilistic method for classifying drought characteristics under a given threshold (Mesbahzadeh et al., 2020; Yevjevich, 1967). Attributes measured through this method include duration, which is the length of time SPEI/SPI values are under a threshold, and frequency, defined as the number of drought events in a period.

3. Results

3.1 Historical Comparison and Validation

To assess the validity of the NEX-GDDP output, historical model output was compared with observed data from the gridMET database. Historical time-series gridded data was aggregated and scaled to allow comparison with the model output. Though all models were compared with the historical time series, the ensemble mean was used as it showed the highest overall geographical accuracy between variables. Figure 2 shows the agreement between model output and historical observation for precipitation, maximum temperature, and potential evapotranspiration. Precipitation showed the least agreement as correlations were low and largely insignificant, while the standard deviation was high across the study site (Appendix 1). This was not unexpected as precipitation is often the hardest variable for GCMs to model and usually shows significant inter- and intra-model variability (Crawford et al., 2019). In contrast, temperature exhibited a high level of agreement with observations. Interestingly, the geographic distribution of this agreement varied among variables. Precipitation demonstrated the strongest alignment with observations on the inland, eastern edge of the study site, whereas temperature and PET exhibited greater conformity in the coastal regions. This observation may speak to the divergent effects of coastal mediation on climatic variables. For example, the high heat capacity of water partially moderates air temperatures, leading to less temporal variability and pronounced extremes while high coastal humidity might complicate precipitation calculations.

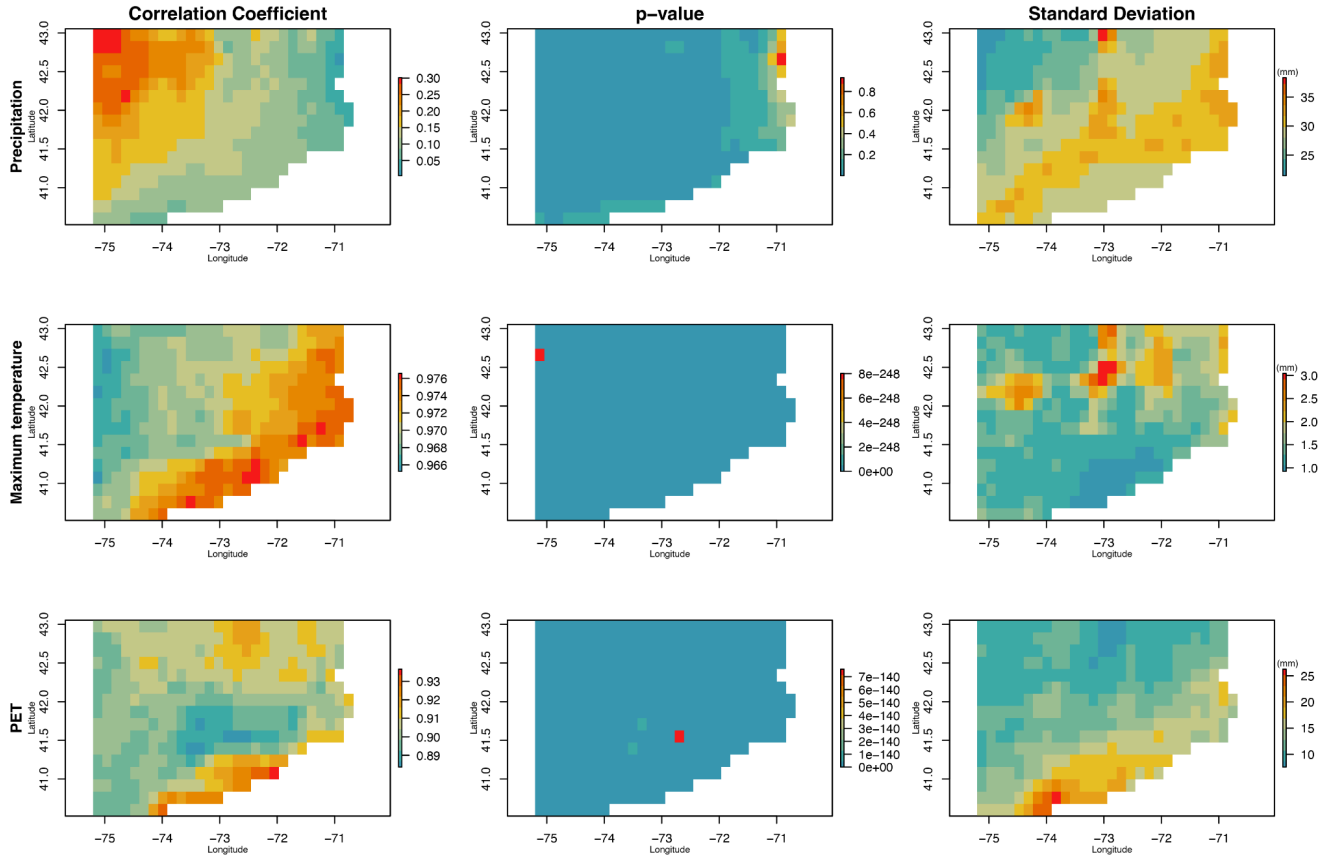


Figure 2. Geographic distribution and historical observation agreement for key variables. Precipitation, maximum temperature, and potential evapotranspiration (PET) are shown in the first, second, and third rows, respectively. The correlation coefficient, significance level, and standard deviation between historical observations and the model output are shown in the first, second, and third columns, respectively.

Due to the relatively high variability in precipitation, bias correction was considered on top of that already performed on the NEX-GDDP dataset using BCSD. To do so, the ISI-MIP approach outlined in Hempel et al. (2013) was employed using an R script developed by Vicedo-Cabrera et al. (2019). This approach was used on the ensemble mean output. Bias-corrected output was then compared with uncorrected model output to assess the improvement (Figure 3). The standard deviation in radiation and precipitation model output was lower than that observed, and though the additional calibration step brought deviation into better agreement, there was little effect on correlation. Though precipitation’s correlation was relatively

poor here, this finding, as previously mentioned, is not uncommon for GCM output (Crawford et al., 2019). Importantly, the magnitude of model output and historical observation were in close agreement, with similar mean values over time (Appendix 1). Finally, bias correction was not utilized for temperature as there appeared to be a tradeoff between decreased correlation and increased standard deviation following the ISI-MIP step. Given the relatively insignificant benefits accorded by the additional bias correction step, the original NEX-GDDP output was in the subsequent analyses.

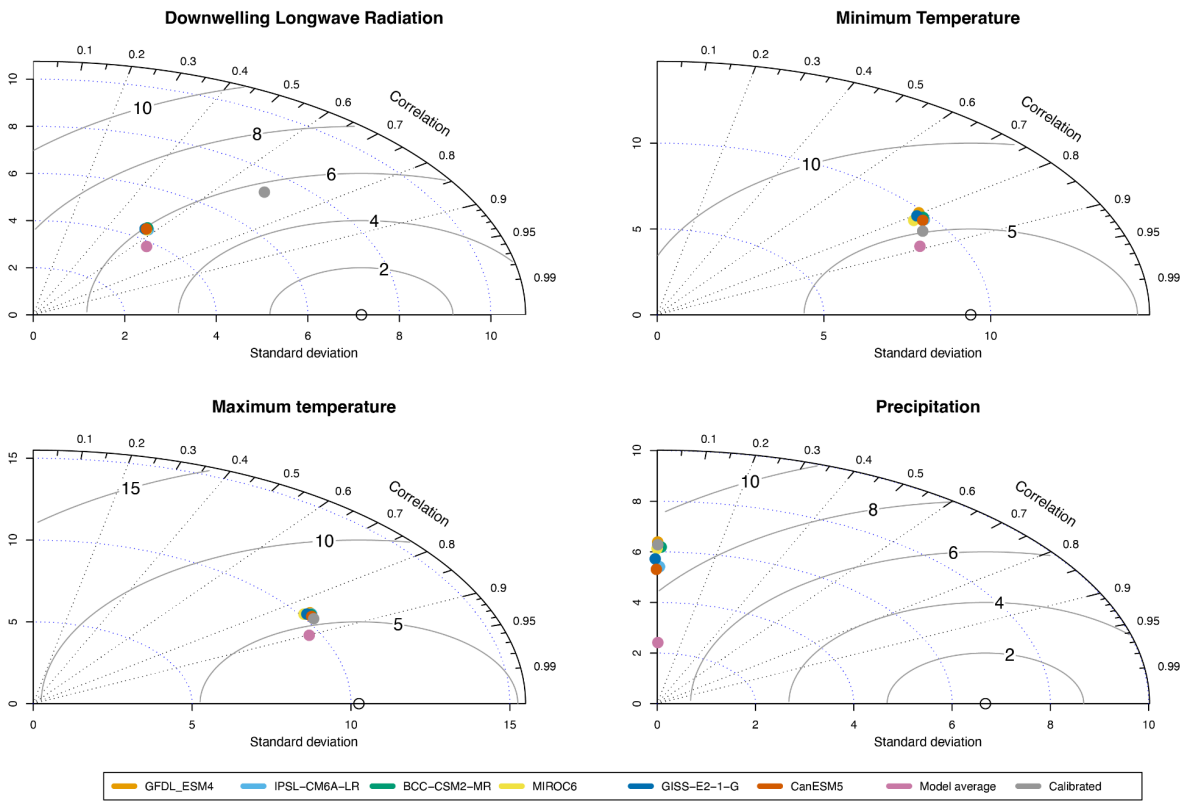


Figure 3. Taylor diagrams showing the agreement between individual models, the model average, and bias-corrected output with historical observations for key variables. Historical observations are marked by the hollow point along the horizontal axis. The standard deviation of output is shown on both the horizontal and vertical axes. The correlation between model output and observation is shown by the location along the major arc. The contours emanating from the point signifying historical observation signify the root-mean-square error (RMSE).

3.2 Long-term SPI and SPEI Record

SPI and SPEI were projected for the years 2015-2100 for SSP1-2.6 and SSP5-8.5 at 1, 6, and 12-month timescales. The sensitivity of the timescale under analysis for trends of a given duration was clearly visible (Figure 4). SPEI calculated at one-month intervals (SPEI-1), the finest resolution projected here, showed relatively little signal over time, while longer-term trends were clearer at the SPEI-6 and SPEI-12 timescales. Considerable variation between models was evident for the metrics across time points, though this variation was generally related to the magnitude of changes rather than their direction. For further analysis, the 6-month and 12-month timescales were chosen because they better reflect the longer-term consequences of drought this study aims to consider.

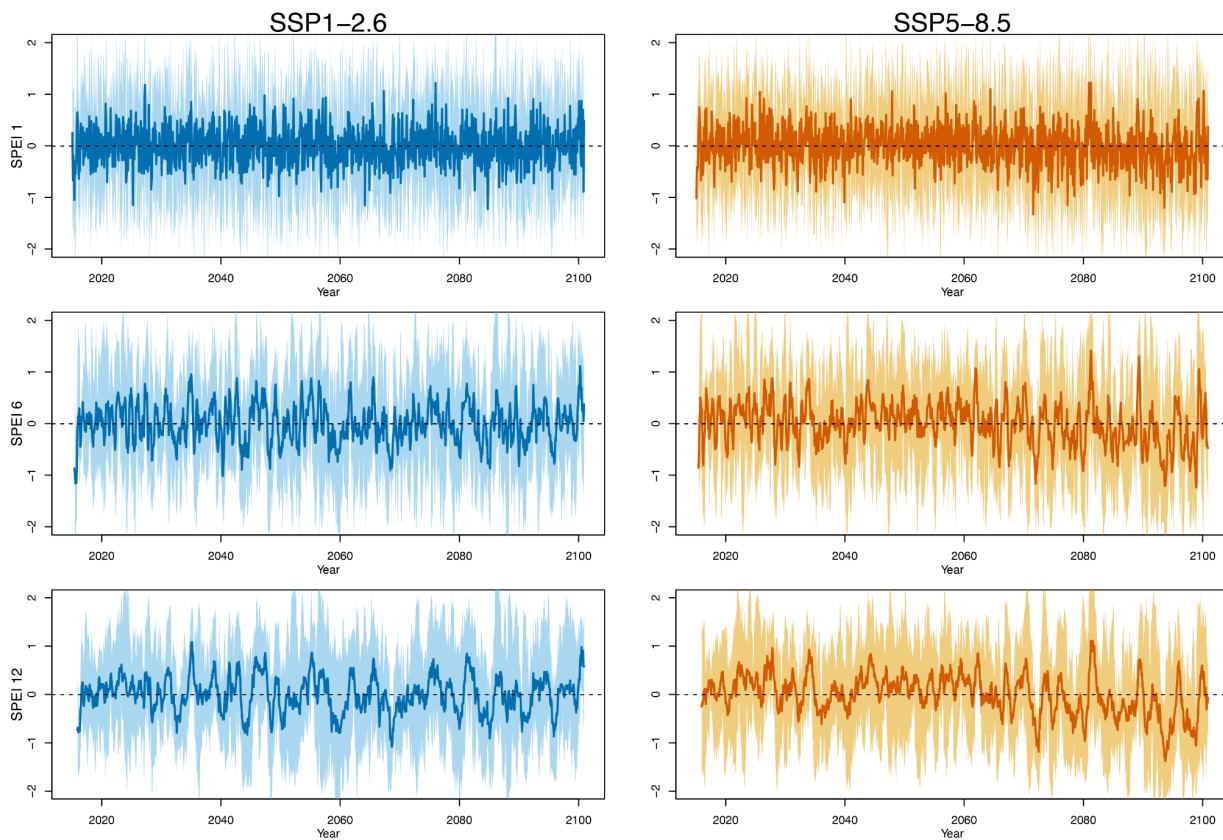


Figure 4. Projections of SPEI at 1, 6, and 12-month time scales. The range of individual model outputs is shown by the shaded region in each figure, and the ensemble average is signified by the darker, single line.

SPI and SPEI showed better agreement under the SSP1-2.6 scenario than the SSP5-8.5 scenario (Figure 5). Under the low emissions SSP1-2.6 scenario, both metrics were strongly associated throughout the study period with only slight disagreement from ~2015-2025, signifying that precipitation is playing the dominant role in drought assessment under this scenario. Under the high emissions SSP5-8.5 scenario, the metrics diverged through the earliest and latest periods. SPEI demonstrated lower values (indicating less water in the system) than SPI at the latter end of the period for both the 6-month and 12-month resolutions. This is most likely the result of PET's inclusion in SPEI's water balance, reflecting the increased evaporative effect expected under warmer climate conditions. This difference affirms SPEI's use as the metric of choice in this study as the effect of warming on long-term drying trends would not otherwise be seen if solely precipitation-based indices were used and encourages its usage in future studies. It should also be noted that SPI has lower values than SPEI across the earlier half of the study period for both time scales and emissions scenarios, with a more pronounced effect under SSP5-8.5, which is somewhat unexpected given the evaporative loss included in SPEI.

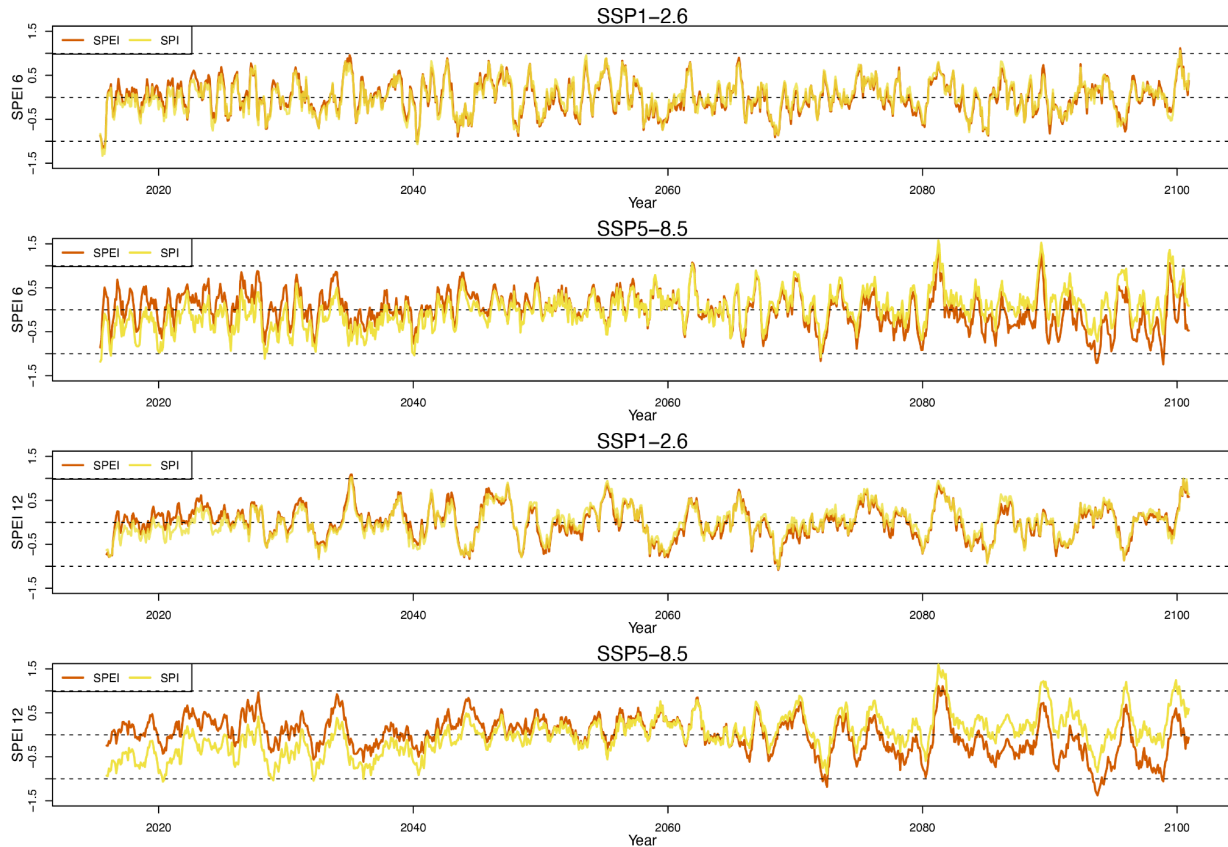


Figure 5. Comparison of SPI and SPEI at 6-month and 12-month timescales for SSP1-2.6 and SSP5-8.5 emissions scenarios. SPEI is shown by the dark orange line and SPI by the yellow line in each. The broken lines mark values at 0, 1, and -1, with the latter being the threshold for moderate drought severity.

3.3 Drought Frequency and Magnitude Increase Over Time

To better assess how drought indices evolve, the severity of their magnitudes was grouped into three categories: moderate ($-1.5 \leq \text{SPEI} \leq -1$), severe ($-2 \leq \text{SPEI} \leq -1.5$), and extreme ($\text{SPEI} \leq -2$). Figure 6a shows the number of months during which drought was present for at least three months in each category between 2015-2057 and 2058-2100 for SPEI-6 and SPEI-12. Both timescales showed nearly identical trends. SSP1-2.6 demonstrated a higher incidence of moderate drought from 2015-2057 than did SSP5-8.5. Significant increases in all severity categories were seen in the high-emissions scenario across the century, with especially

large increases in severe and extreme drought at both timescales. The only decrease between the two intervals was for extreme drought under the SSP1-2.6 scenario, but this effect was moderate.

Results were generally similar for the average drought durations (Figure 6b). Few significant changes in either direction were observed under the low emissions scenario. Notably, SPEI-6 severe drought decreased between periods while SPEI-12 drought increased. Significant increases in drought duration were observed for all three categories under the SSP5-8.5 scenario, especially increases in extreme drought. The magnitude of durations shown by the earlier period of the low emissions scenario in Figure 6b match those of the historical record quite well. The frequency, however, could not be compared with the observational record as the gridMET data series starts in 1979 and therefore does not provide a comparable 42-year span. Overall, these results indicate that the effects of increased evaporation during warming periods are not only significant but also exhibit diverse temporal patterns. The consistent trends in drought across different timescales suggest various impacts on water balance dynamics.

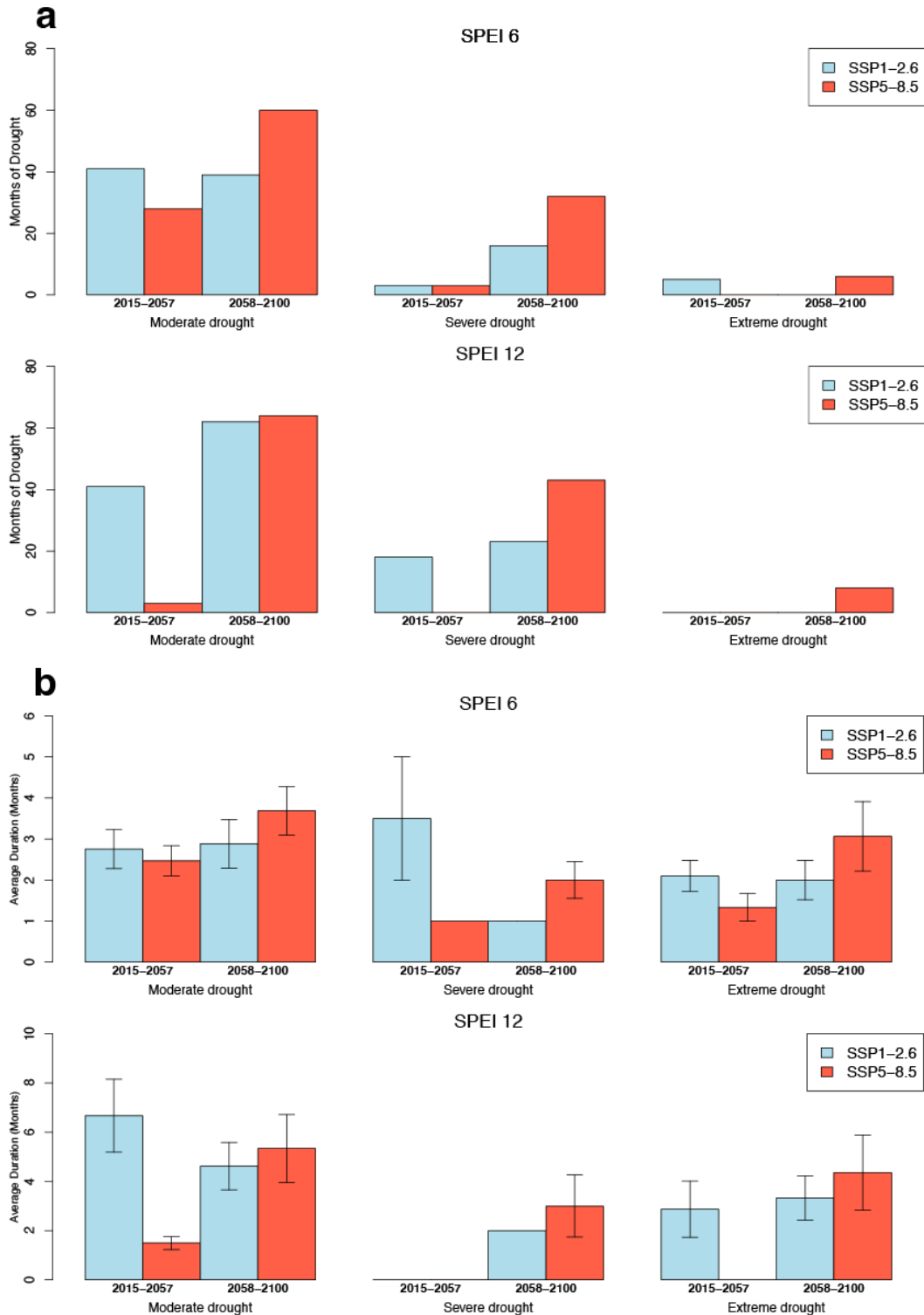


Figure 6. Characteristics of drought for given emissions scenario and time period. The time period is noted below. **(a)** Drought frequency, calculated as the number of drought events within a given period, is shown for each severity category. **(b)** The average drought duration across the drought events, with mean error bars. Category thresholds were determined using the ranges suggested by the WMO (2012). For each category, results from emissions scenarios are split into a 2015-2057 period and a 2058-2100 period.

3.4 Geographic Spread of Drought

Mapping the SPEI shows the geographical variation in drought impacts. Figure 7 segments the total number of months of drought (of duration longer than three months) by emissions scenario, time period, and SPEI resolution. The range of the most drought-prone regions differs significantly between scenario, time, and metric. As is shown in Figure 6, the spatial extent and mean duration of drought are longer during the 2015-2057 period under SSP1-2.6. Regions such as southern Connecticut and Long Island show nearly twice the incidence of drought under this emissions scenario over the earlier time period. Overall, geographic patterns of drought are roughly congruent between the 6-month and 12-month time intervals, with drought spanning the Northwest-Southeast diagonal for SSP1-2.6 and Southern/coastal regions for SSP5-8.5.

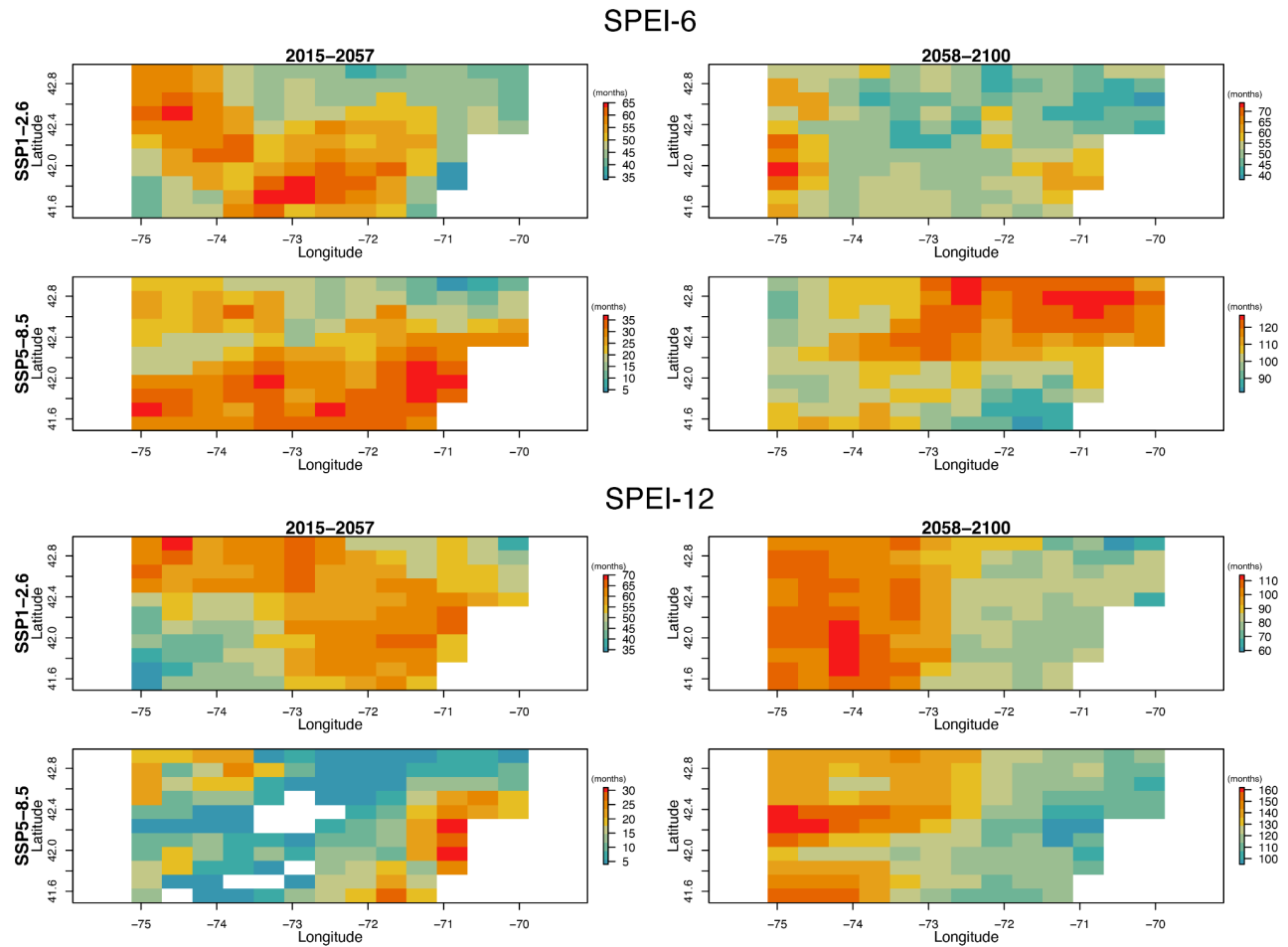


Figure 7. The geographic distribution of drought frequency calculated using SPEI-6 and SPEI-12. The left column displays projections from 2015-2057 and the right from 2058-2100. For each figure, a legend with a color scale is displayed to the right.

Under all measures, drought was more frequent and spanned a wider geographic range under SSP5-8.5. Every grid cell experienced a consistent increase in the number of months experiencing drought conditions across the century. This involves a nearly fourfold increase in frequency in the most drought-prone regions. No regions under this scenario saw decreased drought frequency. SSP1-2.6, conversely, has some sectors in which drought incidence decreases, though many areas stay roughly similar throughout the century. The geographic reach of SPEI-6 drought increased between the periods under SSP1-2.6, with 89.6% of grid cells

experiencing more months of drought in the latter half of the century. All grid cells under SSP1-2.6 experienced increases in drought under SPEI-12, suggesting late-term drought might accumulate over longer time scales under a low emissions scenario. As is also shown in Figures 6 and 7, drought severity shows trends identical to that of drought frequency. The regions that see the largest rise tend to be on the eastern end of the study area, possibly due to less coastal climate mediation. The one exception to this trend appears to be the SPEI-6 measure under SSP5-8.5, in which drought incidence moves to the Northeast corner of the study area.

It is especially interesting to compare the distribution and frequency of drought between emissions scenarios in the early period. SSP1-2.6, somewhat surprisingly, shows a higher incidence of drought across a larger area than SSP5-8.5. The increase in drought in the high emissions scenario throughout the century, however, is substantially larger. These results suggest that the benefits of emissions reductions within the study area might not be seen in the first half of the century, but that these benefits could be substantial in the longer term. These findings also point to the complex impacts of warming on the climate system seen here. The high emissions scenario, following the SPEI results here, will likely increase precipitation in the near future over a low emissions context, before shifting to a substantially greater water deficit. It is hard to unpack how much of this shift is driven by diminished precipitation as opposed to increased evaporation—though if the relatively unchanged SPI values (Figure 5) at the end of the century are a guide, it is most likely the latter. In either case, the high emissions scenario has the possibility of a drought *whiplash*, in which a relative water surplus in the near term greatly decreases towards the end of the century.

4. Discussion

CMIP6 output downscaled and bias-corrected under NEX-GDDP was shown to have good agreement with historical observations. In terms of measured variables, the modeled temperature performance was very high. Precipitation, though reflecting the magnitude of rainfall well, diverged in its correlation and agreement with historical patterns. Derived variables such as potential evapotranspiration showed very high agreement. These findings are similar to those of past studies aimed at assessing variable agreement from GCM model output (Crawford et al., 2019; John et al., 2022). Further, the basic bias correction provided in the NEX-GDDP dataset demonstrates adequate improvements for long-term projection studies. Additional bias correction methods, such as the ISI-MIP method, do not provide significant improvements over that included in the NEX-GDDP dataset.

We found that long-term changes were better reflected in drought indices across longer temporal resolutions (6-month and 12-month) than shorter (1-month), suggesting that future drought might accumulate at deeper water levels. As SPI and SPEI showed better agreement across SSP1-2.6, the low emissions scenario, precipitation may be a dominant driver of water balance levels if radiative forcing is kept low. Under SSP5-8.5, the high emissions scenario, SPEI values negatively diverged from SPI in the second half of the century, especially for SPEI-12. Thus, there appears to be a possible shift in the relative importance of evaporation over precipitation for determining water balances as emissions increase. Interestingly, SPEI values are more positive than SPI in the first half of the century. This was surprising given that one would expect the inclusion of evaporation into the index computation to have an overall lowering effect. Further work should be done to unpack whether this effect is indicative of the statistical approach

used in each metric's calculation or if these differences are reflective of actual meteorological mechanisms.

These results also lead to the unexpected finding that some regions in the study area could experience a marginally higher frequency of moderate and extreme drought in the near future under the low emissions scenario than in the late-term. This contrasts with the high emissions scenario in which all regions experience increases in the frequency of all drought categories. Since the values between time points are quite similar, it's feasible that this trend happened by chance. However, this seems unlikely given the similar pattern produced in the output from individual models, all of which were run independently (Appendix 2). It also seems unlikely that changes in precipitation produce this finding. Overall mean rates and the frequency of extreme precipitation events do not change significantly from the early period to the late period of study under SSP1-2.6, nor does precipitation output differ substantially between emissions scenarios (Appendix 3). Most likely, this finding is driven by moderately higher daily minimum temperatures in the early half of the period under SSP1-2.6 (Appendix 3). Though temperatures under SSP5-8.5 greatly exceed the low emissions scenario by the end of the century, somewhat higher minimum temperatures could lead to higher near-term evaporation rates.

Together, these results suggest that the full benefits of climate change mitigation might not be seen until the latter half of the century. The impacts of such mitigation, however, appear significant. The frequency and duration of moderate, severe, and extreme droughts increase decidedly through the 21st century under SSP5-8.5. The arrival of extreme droughts under both SPEI-6 and SPEI-12 is especially worrisome, given the prior lack of such events and the double temporal scales at which the effects of drought accumulate. Further, these events increase in

frequency across all grid cells in the modeled study area under a high emissions scenario, especially those on the eastern end. Under low emissions, the frequency of all flood events increases across >70% of grid cells, with the exception of extreme droughts for SPEI-6 which experience a moderate decrease in 51% of grid cells. The range of these impacts is notable in its span, and cause for direct consideration.

Thus far, no other studies have performed high resolution SPEI projections using CMIP6 output for this region. Wang et al. (2021) and Zeng et al. (2022) performed global SPEI projections using CMIP6 output, albeit at much coarser resolutions ($2.5^{\circ} \times 2.5^{\circ}$ and $1^{\circ} \times 1^{\circ}$, respectively). These studies found that the study area here would experience small-to-negligible increases in drought frequency and duration. This disagreement was possibly due to the resolution discrepancy between these studies and the work presented here since local water balances might exhibit somewhat substantial changes when downscaled. There is also the possibility, however, that some of these findings are an artifact of the BCSD method used for downscaling and bias correction. As such, further projections should be performed as alternatively downscaled CMIP6 data becomes available.

5. Conclusion

This study has developed long-term projections of drought from CMIP6 output at a higher resolution ($0.25^\circ \times 0.25^\circ$) than has been done in prior research. Further, the SPEI projections here are the first for this region using CMIP6 output. Through this work, we have developed an approach to drought projection from the downscaled NEX-GDDP dataset. The same methods used here can be utilized in future studies with much wider geographic ranges, such as projections across the continental U.S. or the globe. Further, the improved resolution of this study allows for new insights into how SPI/SPEI differ across geographic ranges and provides additional utility for fields that require higher resolutions, such as Public Health and agricultural management. This work also serves as additional verification of CMIP6 output, as well as emphasizes the contributions of NEX-GDDP to climate modeling applications.

Our findings affirm the need for rapid climate change mitigation. Under a high emissions scenario, we found the frequency, severity, and duration of all categories of drought to increase across the entire study region, likely due to heightened evapotranspiration. These increases were significantly greater in magnitude and duration than those experienced under a comparable low-emissions scenario. Further, drought projections across SPEI calculated at 6-month and 12-month timescales showed substantial agreement, suggesting that drought impacts will be multifarious. The benefits from the climate mitigation scenario, however, were largely not seen until the latter half of the century (2058-2100). Accordingly, urgent actions must be taken on emissions reduction to avoid substantial adverse impacts of anthropogenic climate in the latter half of the century.

Acknowledgments

I would like to thank my advisor, Professor Kai Chen, for his support and endlessly thoughtful guidance throughout this process. I am also grateful to my Dean of Undergraduate Studies, Professor Pincelli Hull, for her mentorship and encouragement throughout my time at Yale—my undergraduate experience would not be the same without her. For introducing me to research and showing me what it means to be ceaselessly curious, I would like to thank Professor Mark Brandon. Finally, I am thankful to the residents of 446 Elm St. for their friendship and support this past year.

References

- Abatzoglou, J.T., 2013. Development of gridded surface meteorological data for ecological applications and modelling. *Int. J. Climatol.* 33, 121–131.
<https://doi.org/10.1002/joc.3413>
- Alley, W.M., 1984. The Palmer Drought Severity Index: Limitations and Assumptions. *J. Appl. Meteorol. Climatol.* 23, 1100–1109.
[https://doi.org/10.1175/1520-0450\(1984\)023<1100:TPDSIL>2.0.CO;2](https://doi.org/10.1175/1520-0450(1984)023<1100:TPDSIL>2.0.CO;2)
- Ault, T.R., 2020. On the essentials of drought in a changing climate. *Science* 368, 256–260.
<https://doi.org/10.1126/science.aaz5492>
- Ault, T.R., Mankin, J.S., Cook, B.I., Smerdon, J.E., 2016. Relative impacts of mitigation, temperature, and precipitation on 21st-century megadrought risk in the American Southwest. *Sci. Adv.* 2, e1600873. <https://doi.org/10.1126/sciadv.1600873>
- Bower, E., Meneghetti, L., O'Connor, K., 2015. Global estimates 2015 People displaced by disasters. *Intern. Displac. Monit. Cent. Nor.*
- Center For International Earth Science Information Network-CIESIN-Columbia University, 2018. Population Estimation Service, Version 3 (PES-v3).
<https://doi.org/10.7927/H4DR2SK5>
- Cook, B.I., Cook, E.R., Smerdon, J.E., Seager, R., Williams, A.P., Coats, S., Stahle, D.W., Díaz, J.V., 2016. North American megadroughts in the Common Era: reconstructions and simulations. *WIREs Clim. Change* 7, 411–432. <https://doi.org/10.1002/wcc.394>
- Cook, B.I., Mankin, J.S., Marvel, K., Williams, A.P., Smerdon, J.E., Anchukaitis, K.J., 2020. Twenty-First Century Drought Projections in the CMIP6 Forcing Scenarios. *Earths Future* 8, e2019EF001461. <https://doi.org/10.1029/2019EF001461>

- Crawford, J., Venkataraman, K., Booth, J., 2019. Developing climate model ensembles: A comparative case study. *J. Hydrol.* 568, 160–173.
<https://doi.org/10.1016/j.jhydrol.2018.10.054>
- Droogers, P., Allen, R.G., 2002. Estimating Reference Evapotranspiration Under Inaccurate Data Conditions. *Irrig. Drain. Syst.* 16, 33–45. <https://doi.org/10.1023/A:1015508322413>
- Feng, K., Su, X., 2019. Spatiotemporal Characteristics of Drought in the Heihe River Basin Based on the Extreme-Point Symmetric Mode Decomposition Method. *Int. J. Disaster Risk Sci.* 10, 591–603. <https://doi.org/10.1007/s13753-019-00241-1>
- Haile, G.G., Tang, Q., Hosseini-Moghari, S.-M., Liu, X., Gebremicael, T.G., Leng, G., Kebede, A., Xu, X., Yun, X., 2020. Projected Impacts of Climate Change on Drought Patterns Over East Africa. *Earths Future* 8, e2020EF001502.
<https://doi.org/10.1029/2020EF001502>
- Hargreaves, G.H., 1994. Defining and Using Reference Evapotranspiration. *J. Irrig. Drain. Eng.* 120, 1132–1139. [https://doi.org/10.1061/\(ASCE\)0733-9437\(1994\)120:6\(1132\)](https://doi.org/10.1061/(ASCE)0733-9437(1994)120:6(1132))
- Hargreaves, G.L., Hargreaves, G.H., Riley, J.P., 1985. Agricultural Benefits for Senegal River Basin. *J. Irrig. Drain. Eng.* 111, 113–124.
[https://doi.org/10.1061/\(ASCE\)0733-9437\(1985\)111:2\(113\)](https://doi.org/10.1061/(ASCE)0733-9437(1985)111:2(113))
- Hempel, S., Frieler, K., Warszawski, L., Schewe, J., Piontek, F., 2013. A trend-preserving bias correction – the ISI-MIP approach. *Earth Syst. Dyn.* 4, 219–236.
<https://doi.org/10.5194/esd-4-219-2013>
- Jang, S., Kavvas, M.L., 2015. Downscaling Global Climate Simulations to Regional Scales: Statistical Downscaling versus Dynamical Downscaling. *J. Hydrol. Eng.* 20, A4014006.
[https://doi.org/10.1061/\(ASCE\)HE.1943-5584.0000939](https://doi.org/10.1061/(ASCE)HE.1943-5584.0000939)

- John, A., Douville, H., Ribes, A., Yiou, P., 2022. Quantifying CMIP6 model uncertainties in extreme precipitation projections. *Weather Clim. Extrem.* 36, 100435.
<https://doi.org/10.1016/j.wace.2022.100435>
- Kottek, M., Grieser, J., Beck, C., Rudolf, B., Rubel, F., 2006. World Map of the Köppen-Geiger climate classification updated. *Meteorol. Z.* 15, 259–263.
<https://doi.org/10.1127/0941-2948/2006/0130>
- Kumar, R., Musuza, J.L., Van Loon, A.F., Teuling, A.J., Barthel, R., Ten Broek, J., Mai, J., Samaniego, L., Attinger, S., 2016. Multiscale evaluation of the Standardized Precipitation Index as a groundwater drought indicator. *Hydrol. Earth Syst. Sci.* 20, 1117–1131.
<https://doi.org/10.5194/hess-20-1117-2016>
- Leelaruban, N., Padmanabhan, G., Oduor, P., 2017. Examining the Relationship between Drought Indices and Groundwater Levels. *Water* 9, 82. <https://doi.org/10.3390/w9020082>
- Leeper, R.D., Bilotta, R., Petersen, B., Stiles, C.J., Heim, R., Fuchs, B., Prat, O.P., Palecki, M., Ansari, S., 2022. Characterizing U.S. drought over the past 20 years using the U.S. drought monitor. *Int. J. Climatol.* 42, 6616–6630. <https://doi.org/10.1002/joc.7653>
- Leng, G., Tang, Q., Rayburg, S., 2015. Climate change impacts on meteorological, agricultural and hydrological droughts in China. *Glob. Planet. Change* 126, 23–34.
<https://doi.org/10.1016/j.gloplacha.2015.01.003>
- Long, J., Siu, H., 2018. Refugees from Dust and Shrinking Land: Tracking the Dust Bowl Migrants. *J. Econ. Hist.* 78, 1001–1033. <https://doi.org/10.1017/S0022050718000591>
- Mallya, G., Mishra, V., Niyogi, D., Tripathi, S., Govindaraju, R.S., 2016. Trends and variability of droughts over the Indian monsoon region. *Weather Clim. Extrem.* 12, 43–68.
<https://doi.org/10.1016/j.wace.2016.01.002>

- Masud, B., Cui, Q., Ammar, M.E., Bonsal, B.R., Islam, Z., Faramarzi, M., 2021. Means and Extremes: Evaluation of a CMIP6 Multi-Model Ensemble in Reproducing Historical Climate Characteristics across Alberta, Canada. *Water* 13, 737.
<https://doi.org/10.3390/w13050737>
- McKee, T.B., Doesken, N.J., Kleist, J., 1993. The relationship of drought frequency and duration to time scales. Presented at the Proceedings of the 8th Conference on Applied Climatology, California, pp. 179–183.
- Mesbahzadeh, T., Mirakbari, M., Mohseni Saravi, M., Soleimani Sardoo, F., Miglietta, M.M., 2020. Meteorological drought analysis using copula theory and drought indicators under climate change scenarios (RCP). *Meteorol. Appl.* 27, e1856.
<https://doi.org/10.1002/met.1856>
- Mishra, V., Bhatia, U., Tiwari, A.D., 2020. Bias-corrected climate projections for South Asia from Coupled Model Intercomparison Project-6. *Sci. Data* 7, 338.
<https://doi.org/10.1038/s41597-020-00681-1>
- Ngoma, H., Wen, W., Ayugi, B., Babaousmail, H., Karim, R., Ongoma, V., 2021. Evaluation of precipitation simulations in CMIP6 models over Uganda. *Int. J. Climatol.* 41, 4743–4768.
<https://doi.org/10.1002/joc.7098>
- NOAA, 2020. The High Cost of Drought | January 23, 2020 | Drought.gov [WWW Document]. URL <https://www.drought.gov/news/high-cost-drought> (accessed 4.28.24).
- O'Neill, B.C., Tebaldi, C., van Vuuren, D.P., Eyring, V., Friedlingstein, P., Hurtt, G., Knutti, R., Kriegler, E., Lamarque, J.-F., Lowe, J., Meehl, G.A., Moss, R., Riahi, K., Sanderson, B.M., 2016. The Scenario Model Intercomparison Project (ScenarioMIP) for CMIP6. *Geosci. Model Dev.* 9, 3461–3482. <https://doi.org/10.5194/gmd-9-3461-2016>

- Pacsi, A.P., Alhajeri, N.S., Webster, M.D., Webber, M.E., Allen, D.T., 2013. Changing the spatial location of electricity generation to increase water availability in areas with drought: a feasibility study and quantification of air quality impacts in Texas. *Environ. Res. Lett.* 8, 035029. <https://doi.org/10.1088/1748-9326/8/3/035029>
- Palmer, W.C., 1965. Meteorological drought. US Department of Commerce, Weather Bureau.
- Pokhrel, Y., Felfelani, F., Satoh, Y., Boulange, J., Burek, P., Gädeke, A., Gerten, D., Gosling, S.N., Grillakis, M., Gudmundsson, L., Hanasaki, N., Kim, H., Koutroulis, A., Liu, J., Papadimitriou, L., Schewe, J., Müller Schmied, H., Stacke, T., Telteu, C.-E., Thiery, W., Veldkamp, T., Zhao, F., Wada, Y., 2021. Global terrestrial water storage and drought severity under climate change. *Nat. Clim. Change* 11, 226–233. <https://doi.org/10.1038/s41558-020-00972-w>
- Pyarali, K., Peng, J., Disse, M., Tuo, Y., 2022. Development and application of high resolution SPEI drought dataset for Central Asia. *Sci. Data* 9, 172. <https://doi.org/10.1038/s41597-022-01279-5>
- Ramesh, K.V., Goswami, P., 2014. Assessing reliability of regional climate projections: the case of Indian monsoon. *Sci. Rep.* 4, 4071. <https://doi.org/10.1038/srep04071>
- Schrier, G. van der, Briffa, K.R., Jones, P.D., Osborn, T.J., 2006. Summer Moisture Variability across Europe. *J. Clim.* 19, 2818–2834. <https://doi.org/10.1175/JCLI3734.1>
- Schubert, S.D., Suarez, M.J., Pegion, P.J., Koster, R.D., Bacmeister, J.T., 2004. On the Cause of the 1930s Dust Bowl. *Science* 303, 1855–1859. <https://doi.org/10.1126/science.1095048>
- Schwalm, C.R., Anderegg, W.R.L., Michalak, A.M., Fisher, J.B., Biondi, F., Koch, G., Litvak, M., Ogle, K., Shaw, J.D., Wolf, A., Huntzinger, D.N., Schaefer, K., Cook, R., Wei, Y., Fang, Y., Hayes, D., Huang, M., Jain, A., Tian, H., 2017. Global patterns of drought

- recovery. *Nature* 548, 202–205. <https://doi.org/10.1038/nature23021>
- Scorah, H., Sopinka, A., van Kooten, G.C., 2012. The economics of storage, transmission and drought: integrating variable wind power into spatially separated electricity grids. *Energy Econ.* 34, 536–541. <https://doi.org/10.1016/j.eneco.2011.10.021>
- Secci, D., Tanda, M.G., D’Oria, M., Todaro, V., Fagandini, C., 2021. Impacts of climate change on groundwater droughts by means of standardized indices and regional climate models. *J. Hydrol.* 603, 127154. <https://doi.org/10.1016/j.jhydrol.2021.127154>
- Sousa, P.M., Trigo, R.M., Aizpurua, P., Nieto, R., Gimeno, L., Garcia-Herrera, R., 2011. Trends and extremes of drought indices throughout the 20th century in the Mediterranean. *Nat. Hazards Earth Syst. Sci.* 11, 33–51. <https://doi.org/10.5194/nhess-11-33-2011>
- Sugg, M., Runkle, J., Leeper, R., Bagli, H., Golden, A., Handwerger, L.H., Magee, T., Moreno, C., Reed-Kelly, R., Taylor, M., Woolard, S., 2020. A scoping review of drought impacts on health and society in North America. *Clim. Change* 162, 1177–1195. <https://doi.org/10.1007/s10584-020-02848-6>
- Sun, F., Mejia, A., Zeng, P., Che, Y., 2019. Projecting meteorological, hydrological and agricultural droughts for the Yangtze River basin. *Sci. Total Environ.* 696, 134076. <https://doi.org/10.1016/j.scitotenv.2019.134076>
- Swart, N.C., Cole, J.N.S., Kharin, V.V., Lazare, M., Scinocca, J.F., Gillett, N.P., Anstey, J., Arora, V., Christian, J.R., Jiao, Y., Lee, W.G., Majaess, F., Saenko, O.A., Seiler, C., Seinen, C., Shao, A., Solheim, L., von Salzen, K., Yang, D., Winter, B., Sigmund, M., 2019. CCCma CanESM5 model output prepared for CMIP6 ScenarioMIP. <https://doi.org/10.22033/ESGF/CMIP6.1317>
- Tebaldi, C., Knutti, R., 2007. The use of the multi-model ensemble in probabilistic climate

- projections. *Philos. Trans. R. Soc. Math. Phys. Eng. Sci.* 365, 2053–2075.
<https://doi.org/10.1098/rsta.2007.2076>
- Thrasher, B., Wang, W., Michaelis, A., Melton, F., Lee, T., Nemani, R., 2022. NASA Global Daily Downscaled Projections, CMIP6. *Sci. Data* 9, 262.
<https://doi.org/10.1038/s41597-022-01393-4>
- Touma, D., Ashfaq, M., Nayak, M.A., Kao, S.-C., Diffenbaugh, N.S., 2015. A multi-model and multi-index evaluation of drought characteristics in the 21st century. *J. Hydrol., Drought processes, modeling, and mitigation* 526, 196–207.
<https://doi.org/10.1016/j.jhydrol.2014.12.011>
- van Vuuren, D.P., Riahi, K., Moss, R., Edmonds, J., Thomson, A., Nakicenovic, N., Kram, T., Berkhout, F., Swart, R., Janetos, A., Rose, S.K., Arnell, N., 2012. A proposal for a new scenario framework to support research and assessment in different climate research communities. *Glob. Environ. Change* 22, 21–35.
<https://doi.org/10.1016/j.gloenvcha.2011.08.002>
- Vicedo-Cabrera, A.M., Sera, F., Gasparrini, A., 2019. Hands-on Tutorial on a Modeling Framework for Projections of Climate Change Impacts on Health. *Epidemiology* 30, 321.
<https://doi.org/10.1097/EDE.0000000000000982>
- Vicente-Serrano, S.M., Beguería, S., López-Moreno, J.I., 2010. A Multiscalar Drought Index Sensitive to Global Warming: The Standardized Precipitation Evapotranspiration Index. *J. Clim.* 23, 1696–1718. <https://doi.org/10.1175/2009JCLI2909.1>
- Vicente-Serrano, S.M., Beguería, S., Lorenzo-Lacruz, J., Camarero, J.J., López-Moreno, J.I., Azorin-Molina, C., Revuelto, J., Morán-Tejada, E., Sanchez-Lorenzo, A., 2012. Performance of Drought Indices for Ecological, Agricultural, and Hydrological

- Applications. *Earth Interact.* 16, 1–27. <https://doi.org/10.1175/2012EI000434.1>
- Vicente-Serrano, S.M., López-Moreno, J.I., 2005. Hydrological response to different time scales of climatological drought: an evaluation of the Standardized Precipitation Index in a mountainous Mediterranean basin. *Hydrol. Earth Syst. Sci.* 9, 523–533. <https://doi.org/10.5194/hess-9-523-2005>
- Wang, T., Tu, X., Singh, V.P., Chen, X., Lin, K., 2021. Global data assessment and analysis of drought characteristics based on CMIP6. *J. Hydrol.* 596, 126091. <https://doi.org/10.1016/j.jhydrol.2021.126091>
- Wang, W., Wang, J., Romanowicz, R., 2021. Uncertainty in SPI Calculation and Its Impact on Drought Assessment in Different Climate Regions over China. *J. Hydrometeorol.* 22, 1369–1383. <https://doi.org/10.1175/JHM-D-20-0256.1>
- Wells, N., Goddard, S., Hayes, M.J., 2004. A Self-Calibrating Palmer Drought Severity Index. *J. Clim.* 17, 2335–2351. [https://doi.org/10.1175/1520-0442\(2004\)017<2335:ASPDSI>2.0.CO;2](https://doi.org/10.1175/1520-0442(2004)017<2335:ASPDSI>2.0.CO;2)
- Wood, A.W., Leung, L.R., Sridhar, V., Lettenmaier, D.P., 2004. Hydrologic Implications of Dynamical and Statistical Approaches to Downscaling Climate Model Outputs. *Clim. Change* 62, 189–216. <https://doi.org/10.1023/B:CLIM.0000013685.99609.9e>
- World Meteorological Organization, 2012. Standardized precipitation index user guide. *World Meteorol. Organ.* 1090.
- Wu, T., Chu, M., Dong, M., Fang, Y., Jie, W., Li, J., Li, W., Liu, Q., Shi, X., Xin, X., Yan, J., Zhang, F., Zhang, J., Zhang, L., Zhang, Y., 2018. BCC BCC-CSM2MR model output prepared for CMIP6 CMIP historical. <https://doi.org/10.22033/ESGF/CMIP6.2948>
- Yevjevich, V.M., 1967. An objective approach to definitions and investigations of continental

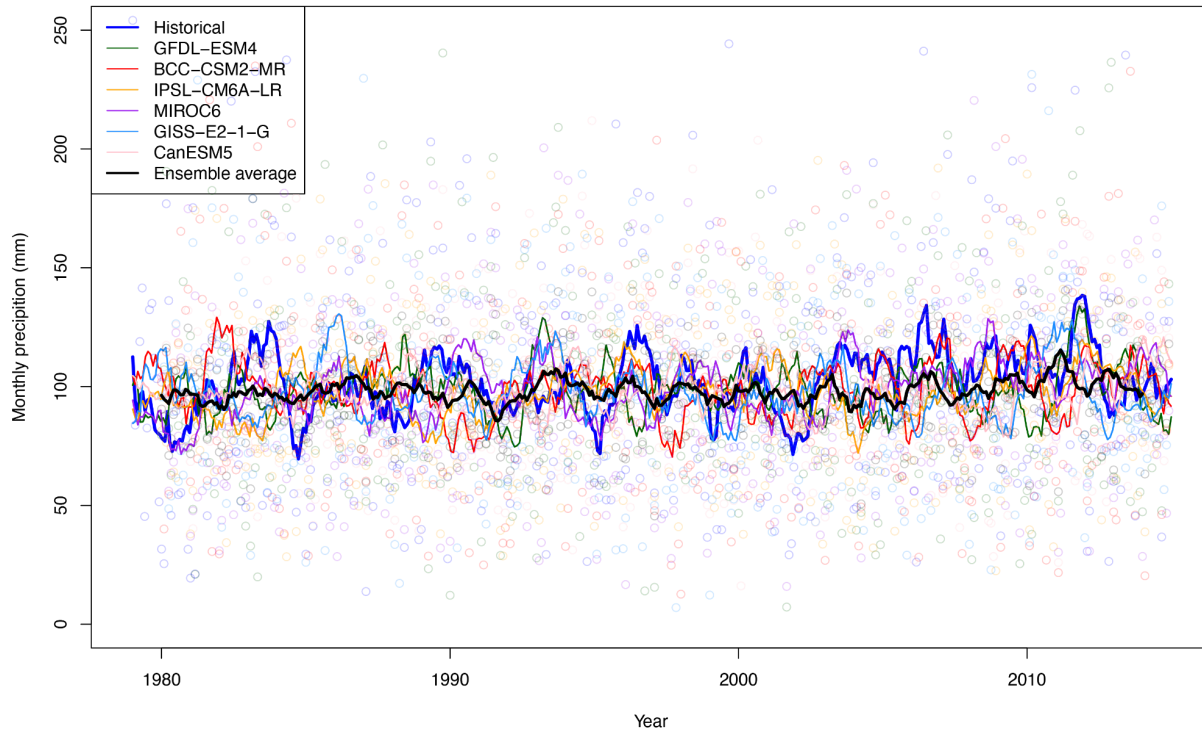
hydrologic droughts. Colorado State University Fort Collins, CO, USA.

Zargar, A., Sadiq, R., Naser, B., Khan, F.I., 2011. A review of drought indices. *Environ. Rev.* 19, 333–349. <https://doi.org/10.1139/a11-013>

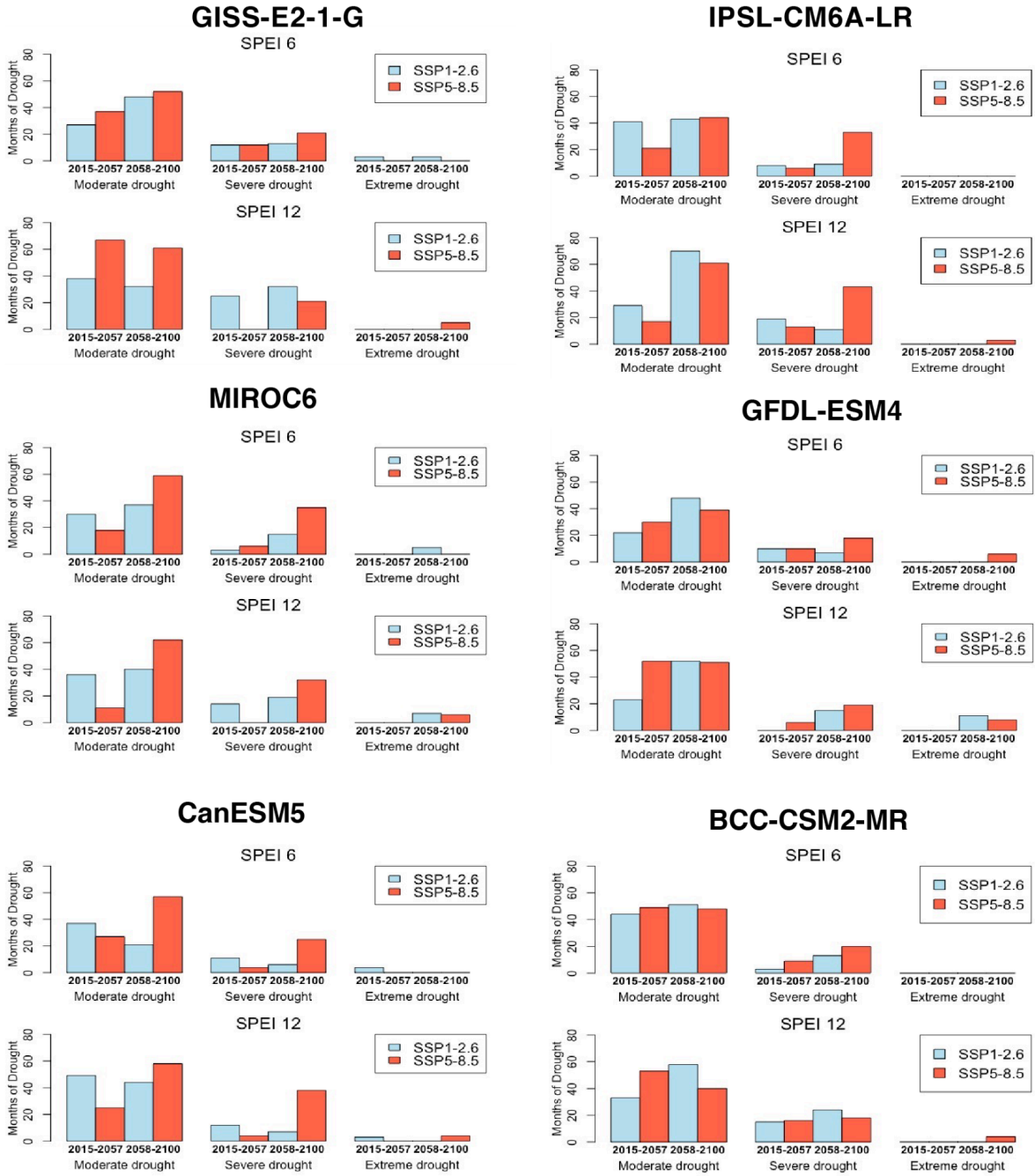
Zeng, J., Li, J., Lu, X., Wei, Z., Shangguan, W., Zhang, Shupeng, Dai, Y., Zhang, Shulei, 2022. Assessment of global meteorological, hydrological and agricultural drought under future warming based on CMIP6. *Atmospheric Ocean. Sci. Lett.*, Center for Climate System Prediction Research (CCSP) 15, 100143. <https://doi.org/10.1016/j.aosl.2021.100143>

Zhang, Q., Shen, Z., Xu, C.-Y., Sun, P., Hu, P., He, C., 2019. A new statistical downscaling approach for global evaluation of the CMIP5 precipitation outputs: Model development and application. *Sci. Total Environ.* 690, 1048–1067. <https://doi.org/10.1016/j.scitotenv.2019.06.310>

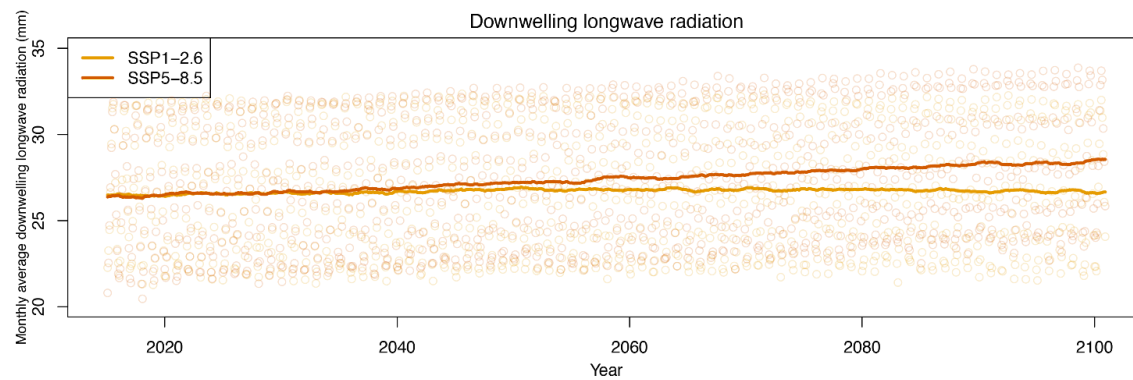
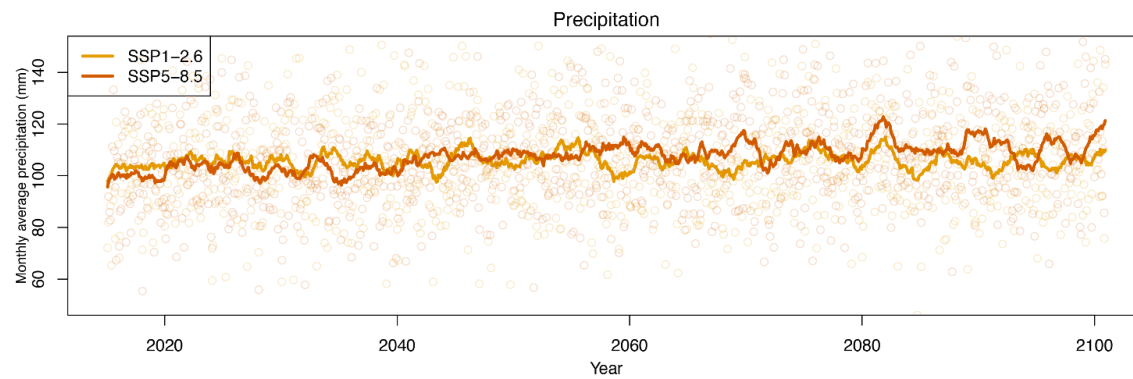
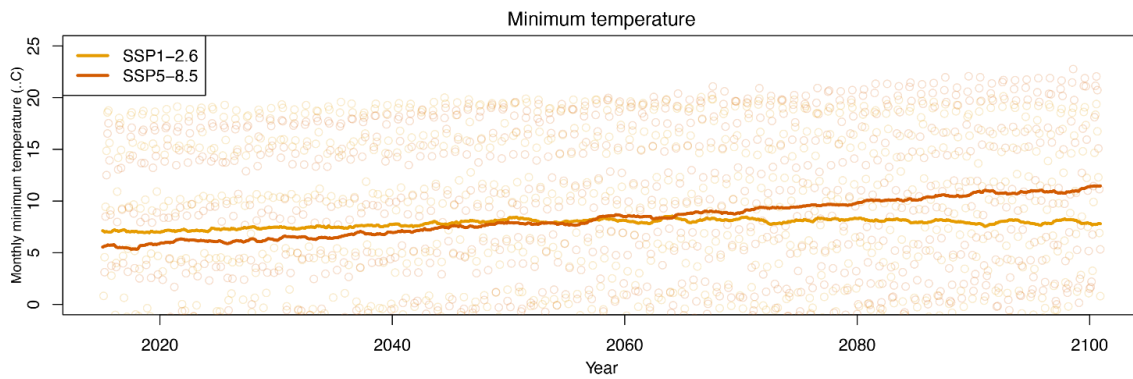
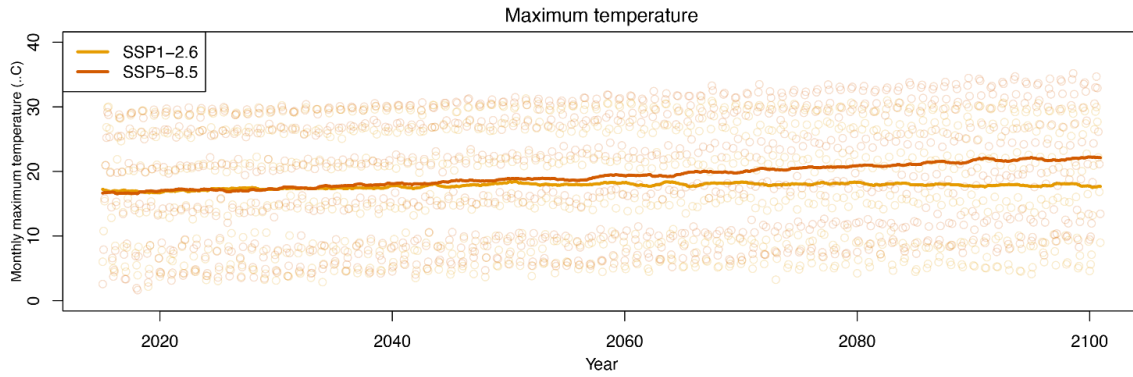
Appendix

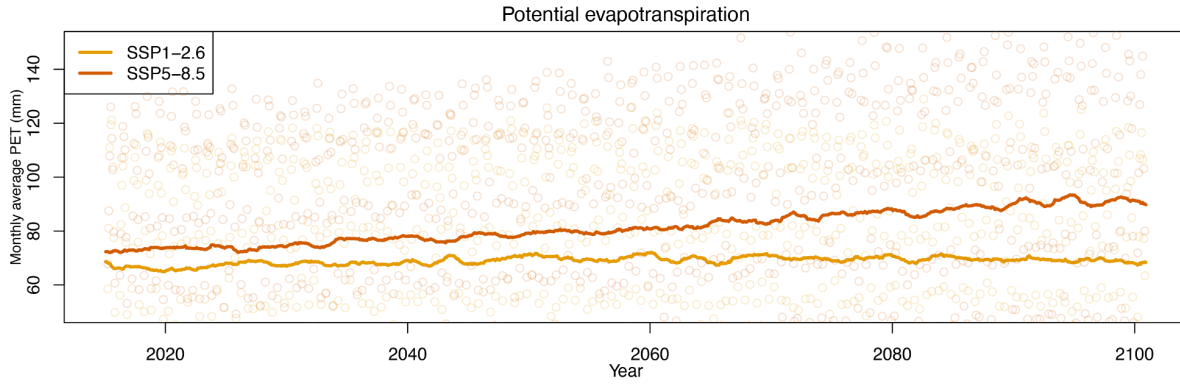


Appendix 1. Monthly precipitation values are shown for historical observations (blue line), individual models, and the ensemble average (black line). Singular values are shown by the individual colored points and a 12-month averaged line shown in the same respective color is shown for each model.



Appendix 2. Projections of drought frequency by severity category for each model considered in this study.





Appendix 3. Long-term projections of maximum and minimum temperature, precipitation, longwave radiation, and potential evapotranspiration. SSP1-2.6 and SSP5-8.5 are shown by the orange and maroon points and lines, respectively.